Since January 2020 Elsevier has created a COVID-19 resource centre with free information in English and Mandarin on the novel coronavirus COVID-19. The COVID-19 resource centre is hosted on Elsevier Connect, the company's public news and information website.

Partial Differential Equations in Applied Mathematics 6 (2022) 100460

Contents lists available at ScienceDirect

Partial Differential Equations in Applied Mathematics

journal homepage: www.elsevier.com/locate/padiff

Numerical study of a nonlinear COVID-19 pandemic model by finite difference and meshless methods

Rahat Zarin

Department of Basic Sciences, University of Engineering and Technology, Peshawar, Khyber Pakhtunkhwa, Pakistan

ARTICLE INFO

Keywords:
Parameter estimation
Real data
Pandemic model
COVID-19
Meshless method

ABSTRACT

In this paper, a mathematical epidemiological model in the form of reaction diffusion is proposed for the transmission of the novel coronavirus (COVID-19). The next-generation method is utilized for calculating the threshold number R_0 while the least square curve fitting approach is used for estimating the parameter values. The mathematical epidemiological model without and with diffusion is simulated through the operator splitting approach based on finite difference and meshless methods. Further, for the graphical solution of the nonlinear model, we have applied a one-step explicit meshless procedure. We study the numerical simulation of the proposed model under the effects of diffusion. The stability analysis of the endemic equilibrium point is investigated. The obtained numerical results are compared mutually since the exact solutions are not available.

1. Introduction

The coronavirus family is a well-known dangerous community of viruses that have caused millions of deaths all over the world. In this family, SARS has infected eight thousand plus infections with more than eight hundred deaths all over the world. Another member is MERS, which spread out from Saudi Arabia to many different countries and affected around 25,000 population in which nearly thousands of humans lost their life. Now recently in December 2019, one more member came called COVID-19 which is first recognized in Wuhan, China.[1] At the start of the new year 2020, this disease started to first spread in China and then all over the world and affected almost 130 million population by today (2nd November). This disease spread out very badly because of specific reasons like the exact treatment along with the vaccine is not present, a high epidemic transmission rate, the exact nature of the virus is not well-known, etc. So today around 210 territories and countries have seen infected by this deadly virus. Currently, lockdown is the common initial action that is taken by all governments to stop the transmission of COVID-19.[2–7] Despite the unavailability of the vaccine and any permanent treatment, the technique worked well by protecting the population from this virus. But the lockdown has given a big economic loss to many countries and they have faced a measurable financial crisis. It has been observed that lockdowns in high-population nations may decrease the transmission rate of the epidemic partially. Also, from the financial loss point of view, such a lockdown cannot be taken for a long time. So at this tough time, it is becoming a tough task to make maintenance between lockdown and financial crash.[8–10]

As per initial medical research, the most general indications of COVID-19 along with the latency period of 11 to 14 days are diarrhea, myalgia, shortness of breath, fever, and cough. The most dangerous of this virus is for those people who are above 60 years old. The transmission rate of this virus is much high and the value basic reproduction number is probably near around 2.2 and 3.58 for a number of countries. That is the reason for its rapid spreading throughout the world and affecting 213 countries. Hence, on 30 January 2020, the world health organization (WHO) announced COVID-19 as one of a global epidemics. One-to-one physical interaction with infected people and respiratory droplets generated from COVID-19 patients are the main reason for transmission.[11–13]

After the big spread of COVID-19 in China, this virus spread out to Iran and Italy. As we know that Iran is a closed country to Pakistan and thousands of population enter Iran for commercial and religious reasons. So after traveling to this nation, when people came back from Iran then some of them were recognized as COVID-19 positive and then they infected many persons in Pakistan. The government restricted travel between these countries but the first positive individual was recognized officially on 26 February 2020, from Karachi, which came back from Iran. So the government ruled out a strict lockdown and suggested the quarantine of infected ones at their home.

Right now, no legitimate and successful treatment is accessible for individuals infected by COVID-19 with the exception of certain medications such as Remdesivir which are endorsed by certain nations like the European Union and Australia.[14] Subsequently, there is no power and approved antibody for this novel contamination albeit not many nations have guaranteed it. The best avoidance methodologies utilized in near nations to diminish and postpone the pandemic pick (straightening everything out) are the successive tests to decide the contaminated people, detachment and lockdown, social separating,

E-mail address: rahat.zarin@uetpeshawar.edu.pk.

https://doi.org/10.1016/j.padiff.2022.100460
Received 12 November 2021; Received in revised form 27 October 2022; Accepted 30 October 2022

utilization of severe SOPs, and so forth until successful medicines and antibodies become accessible. Preventive measures are just the best approach to lessen the shot at diseases and slow the spread of the infection. Analyst all throughout the planet is centering on the plain procedure to conquer the COVID-19 pandemic. For this reason, they have taken on various approaches to investigate the perplexing transmission elements of this contamination. "Numerical models are one of the most impressive instruments in such a manner. Numerous epidemic models were acquainted with investigating the dynamic of COVID-19 and talk about the conceivable control systems for the illness end in various districts of the world. For example, a model of COVID-19 with Lockdown is proposed in Ref. 15, and the effect of undetected cases by means of a numerical model is investigated. The effect of some preventive measures on the abridging of COVID-19 in Pakistan by means of another numerical model is introduced in" Refs. 16, 17. A transmission numerical model considering the ecological spread of the infection with a contextual analysis of Saudi Arabia is concentrated in Refs. 18, 19.

Sources reveal that the virus originated in Huanan and infected the human population through animals.[20] However, evidence is provided by a genomic study where it is considered that from another, yet unknown location, the virus was introduced into the fish market and hence a more rapid spreading started from here.[21] The transmission due to person-to-person interaction is confirmed by infection in clusters of family members and medical workers.[22] After January 1, 2020, statistics show that more than 70% of the patients had no market exposure.[20] It is thought that respiratory droplets due to coughing and sneezing, from an infected person, are the main transmission sources in human-to-human interactions. Up to 96 hours and 9 days persistence of SARS-Cov and other coronaviruses respectively have been recorded and therefore, fomites may also be among the main sources of transmission.[22]

Meshless methods based on Radial Basis Functions (RBFs) appeared frequently in the numerical solution of different physical problems.[23–27] In 1990 Kansa established a collocation method based on MQ RBFs to interpolate random data[27] and to approximate PDEs.[28] The approach caused much fame to the meshless methods due to its meshless nature and handling of complex geometries in higher dimensions. Kansa method is based on global interpolation through RBFs and the existence of non-singularity of the coefficient matrix obtained in Kansa's Method has been comprehensively studied in Refs. 29–31. Some of the researchers used the spectral element method for the PDEs models.[32–35]

2. Formulation of the epidemiological model

In this section, I consider a mathematical epidemiological model for the transmission of COVID-19 pandemic which was recently proposed by M. Mandala et al.[36]

$$\begin{aligned}
\frac{d\mathbb{S}}{dt} &= A - \beta\gamma_1\gamma_2\mathbb{S}\mathbb{E} + b_1\mathbb{Q} - d\mathbb{S}\\
\frac{d\mathbb{E}}{dt} &= \beta\gamma_1\gamma_2\mathbb{S}\mathbb{E} - b_2\mathbb{E} - \alpha\mathbb{E} - \sigma\mathbb{E} - d\mathbb{E}\\
\frac{d\mathbb{Q}}{dt} &= b_2\mathbb{E} - b_1\mathbb{Q} - c\mathbb{Q} - d\mathbb{Q}\\
\frac{d\mathbb{I}}{dt} &= \alpha\mathbb{E} + c\mathbb{Q} - (\eta + d + \delta)\mathbb{I}\\
\frac{d\mathbb{R}}{dt} &= \eta\mathbb{I} + \sigma\mathbb{E} - d\mathbb{R}.
\end{aligned} \tag{2.1}$$

The above model (2.1) expects a homogeneous population, where the population blends in such a path that there is no distinction between individual in one spot and individual in somewhere else. In any case, in genuine situations, the infection may spread quicker in one spot than in another in light of various conditions like diverse climate conditions, and so on Consequently, it is fundamental for the factors to rely upon space too. Subsequently, we extend model (2.1) to the following system:

$$\begin{aligned}
\frac{\partial\mathbb{S}(\mathbb{X},t)}{\partial t} &= A - \beta\gamma_1\gamma_2\mathbb{S}(\mathbb{X},t)\mathbb{E}(\mathbb{X},t) + b_1\mathbb{Q}(\mathbb{X},t) - d\mathbb{S}(\mathbb{X},t) + d_1\frac{\partial^2\mathbb{S}(\mathbb{X},t)}{\partial\mathbb{X}^2}\\
\frac{\partial\mathbb{E}(\mathbb{X},t)}{\partial t} &= \beta\gamma_1\gamma_2\mathbb{S}(\mathbb{X},t)\mathbb{E}(\mathbb{X},t) - (b_2 + \alpha + \sigma + d)\mathbb{E}(\mathbb{X},t) + d_2\frac{\partial^2\mathbb{E}(\mathbb{X},t)}{\partial\mathbb{X}^2}\\
\frac{\partial\mathbb{Q}(\mathbb{X},t)}{\partial t} &= b_2\mathbb{E}(\mathbb{X},t) - b_1\mathbb{Q}(\mathbb{X},t) - c\mathbb{Q}(\mathbb{X},t) - d\mathbb{Q}(\mathbb{X},t) + d_3\frac{\partial^2\mathbb{Q}(\mathbb{X},t)}{\partial\mathbb{X}^2}\\
\frac{\partial\mathbb{I}(\mathbb{X},t)}{\partial t} &= \alpha\mathbb{E}(\mathbb{X},t) + c\mathbb{Q}(\mathbb{X},t) - (\eta + d + \delta)\mathbb{I}(\mathbb{X},t) + d_4\frac{\partial^2\mathbb{I}(\mathbb{X},t)}{\partial\mathbb{X}^2}\\
\frac{\partial\mathbb{R}(\mathbb{X},t)}{\partial t} &= \eta\mathbb{I}(\mathbb{X},t) + \sigma\mathbb{E}(\mathbb{X},t) - d\mathbb{R}(\mathbb{X},t) + d_5\frac{\partial^2\mathbb{R}(\mathbb{X},t)}{\partial\mathbb{X}^2},
\end{aligned} \tag{2.2}$$

the initial conditions for the above model as follows:

$$\begin{aligned}
&\mathbb{S}(\mathbb{X},0) = \Psi_1(\mathbb{X}), \quad \mathbb{E}(\mathbb{X},0) = \Psi_2(\mathbb{X}), \quad \mathbb{I}(\mathbb{X},0) = \Psi_3(\mathbb{X}),\\
&\mathbb{Q}(\mathbb{X},0) = \Psi_4(\mathbb{X}), \quad \mathbb{R}(\mathbb{X},0) = \Psi_5(\mathbb{X})
\end{aligned} \tag{2.3}$$

and with no flux boundary conditions;

$$\begin{aligned}
&\mathbb{S}_{\mathbb{X}}(0,t) = 0, \mathbb{S}_{\mathbb{X}}(Ł,t) = 0, \mathbb{E}_{\mathbb{X}}(0,t) = 0, \mathbb{E}_{\mathbb{X}}(Ł,t) = 0, \mathbb{I}_{\mathbb{X}}(0,t) = 0,\\
&\mathbb{I}_{\mathbb{X}}(Ł,t) = 0, \mathbb{Q}_{\mathbb{X}}(0,t) = 0, \mathbb{Q}_{\mathbb{X}}(Ł,t) = 0, \mathbb{R}_{\mathbb{X}}(0,t) = 0, \mathbb{R}_{\mathbb{X}}(Ł,t) = 0.
\end{aligned} \tag{2.4}$$

3. Equilibrium points and reproductive number R_0

In the absence of disease the equilibrium point called disease free equilibrium (DFE) point. The DFE point for the above model is given as follows:

$$DFE = (\mathbb{S}^0, \mathbb{E}^0, \mathbb{Q}^0, \mathbb{I}^0, \mathbb{R}^0) = \left(\frac{A}{d}, 0, 0, 0, \frac{A}{d^2}\right). \tag{3.1}$$

The endemic equilibrium (EE).

$$\begin{cases}
\mathbb{S}^* = \dfrac{(\alpha + b_2 + d + \sigma)}{\beta\gamma_1\gamma_2},\\
\mathbb{E}^* = \dfrac{(b_1 + c + d)[d(\alpha + b_2 + d + \sigma)(R_0 - 1)]}{\beta\gamma_1\gamma_2[b_2(c + d) + (b_1 + c + d)(\alpha + \sigma + d)]},\\
\mathbb{Q}^* = \dfrac{b_2[(d + pM)(\alpha + b_2 + d + \sigma)(R_0 - 1)]}{\beta\gamma_1\gamma_2[b_2(c + d) + (b_1 + c + d\chi)(\alpha + \sigma + d)]},\\
\mathbb{I}^*\\
= \dfrac{\{\alpha(b_1 + c + d) + b_2c\}[d(\alpha + b_2 + d + \sigma)(R_0 - 1)\}}{\beta(1 - \rho_1)(1 - \rho_2)(b_2(c + d) + (d + \sigma + \alpha)(b_1 + c + d))(\eta + d + \delta)},\\
\mathbb{R}^* = \dfrac{\eta\mathbb{I}^* + \sigma\mathbb{E}^*}{d}.
\end{cases} \tag{3.2}$$

"An illness' spread and control are linked to the reproduction number R_0. In the event of $R_0 < 1$, the disease eliminates from the population, resulting in a regionally and globally stable state of disease-free equilibrium. In addition, it prevents the spread of an epidemic through prevention. Additionally, if $R_0 > 1$, we have both locally and globally endemic equilibrium, but subject to specific conditions. As a result, diseases persist in populations permanently and become epidemics".[37] The reproductive number R_0 for the above model is given as:

$$R_0 = \frac{A\beta\gamma_1\gamma_2}{d(\alpha + d + \sigma + b_2)}, \tag{3.3}$$

when, $d_1 = 0, d_2 = 0, d_3 = 0, d_4 = 0, d_5 = 0$.

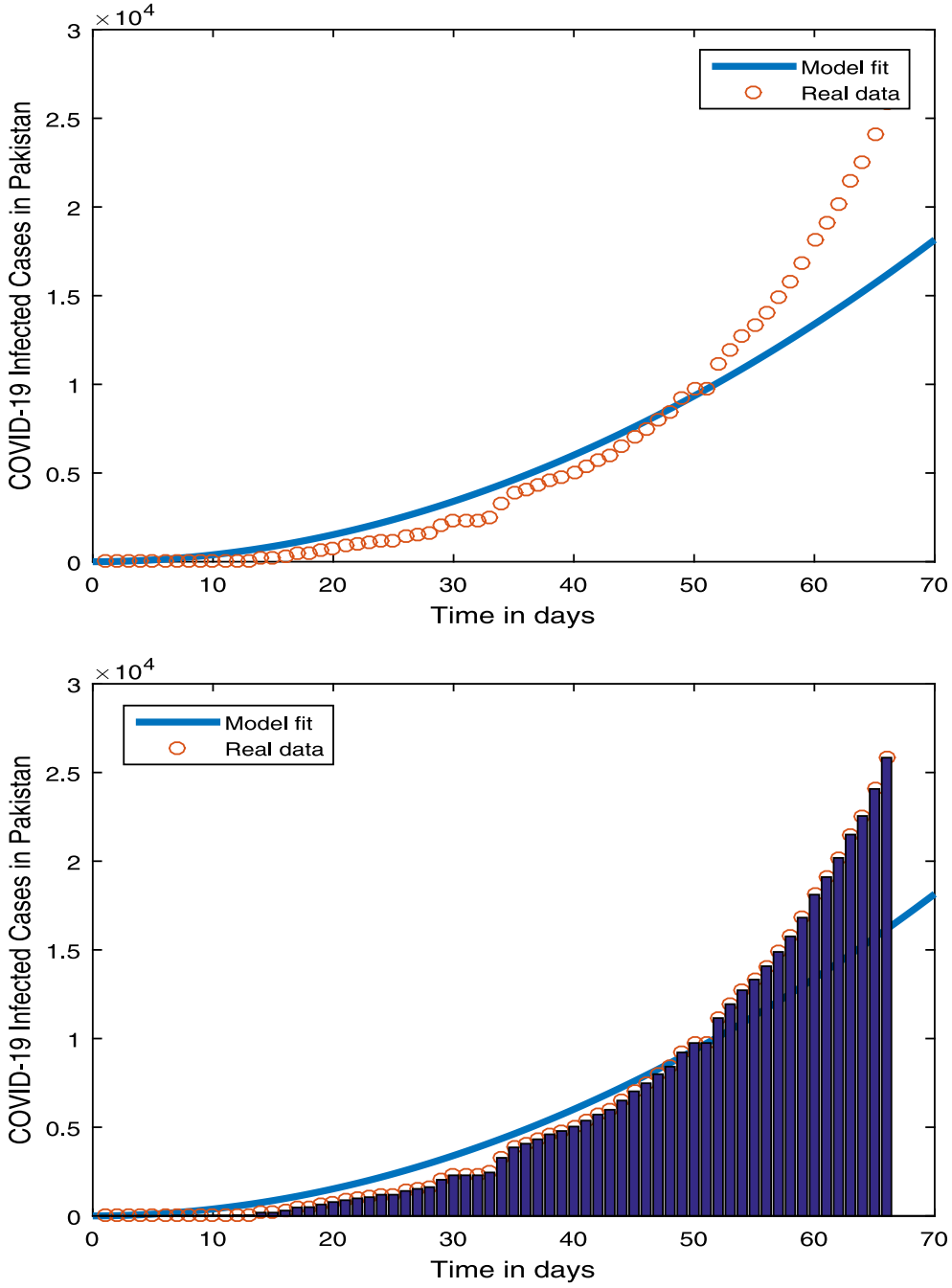

Fig. 1. Confirmed COVID-19 cumulative cases time series in Pakistan[38].

Table 1
Parameters description and estimated values.

Symbols	Description	Values	References
A	Influx rate	1.4057 day^{-1}	Estimated
β	Disease transmission rate	0.0477 day^{-1}	Estimated
δ	COVID-19 induced death rate	0.0005 day^{-1}	Estimated
b_1	Transmission rate from $\mathbb{Q}$ to $\mathbb{S}$	0.0057 day^{-1}	Estimated
b_2	Transmission rate from $\mathbb{E}$ to $\mathbb{Q}$	0.0805 day^{-1}	Estimated
γ_1	Rate of contact from $\mathbb{E}$ to $\mathbb{S}$	0.0876 day^{-1}	Estimated
γ_2	Rate of contact from $\mathbb{S}$ to $\mathbb{E}$	0.0205 day^{-1}	Estimated
α	Transmission rate from $\mathbb{E}$ to $\mathbb{I}$	0.3506 day^{-1}	Estimated
η	Recovery rate infected individuals $\mathbb{I}$	0.1805 day^{-1}	Estimated
d	Natural death rate	0.0009 day^{-1}	Estimated

4. Stability of the SEQIR model at equilibrium point

In order to obtain a small perturbations $\bar{\mathbb{S}}(\mathbb{X},t), \bar{\mathbb{E}}(\mathbb{X},t), \bar{\mathbb{Q}}(\mathbb{X},t), \bar{I}_a(\mathbb{X},t), \bar{\mathbb{R}}(\mathbb{X},t)$, we linearized system (2.2) about E^*, as like in Ref. 39.

$$\begin{aligned}
\frac{\partial \bar{\mathbb{S}}}{\partial t} &= \mathbb{V}_{11}\bar{\mathbb{S}} + \mathbb{V}_{12}\bar{\mathbb{E}} + \mathbb{V}_{13}\bar{\mathbb{Q}} + \mathbb{V}_{14}\bar{\mathbb{I}} + \mathbb{V}_{15}\bar{\mathbb{R}} + d_1\frac{\partial^2 \bar{\mathbb{S}}}{\partial \mathbb{X}^2}\\
\frac{\partial \bar{\mathbb{E}}}{\partial t} &= \mathbb{V}_{21}\bar{\mathbb{S}} + \mathbb{V}_{22}\bar{\mathbb{E}} + \mathbb{V}_{23}\bar{\mathbb{Q}} + \mathbb{V}_{24}\bar{\mathbb{I}} + \mathbb{V}_{25}\bar{\mathbb{R}} + d_2\frac{\partial^2 \bar{\mathbb{E}}}{\partial \mathbb{X}^2}\\
\frac{\partial \bar{\mathbb{Q}}}{\partial t} &= \mathbb{V}_{31}\bar{\mathbb{S}} + \mathbb{V}_{32}\bar{\mathbb{E}} + \mathbb{V}_{33}\bar{\mathbb{Q}} + \mathbb{V}_{34}\bar{\mathbb{I}} + \mathbb{V}_{35}\bar{\mathbb{R}} + d_3\frac{\partial^2 \bar{\mathbb{Q}}}{\partial \mathbb{X}^2}\\
\frac{\partial \bar{\mathbb{I}}}{\partial t} &= \mathbb{V}_{41}\bar{\mathbb{S}} + \mathbb{V}_{42}\bar{\mathbb{E}} + \mathbb{V}_{43}\bar{\mathbb{Q}} + \mathbb{V}_{44}\bar{\mathbb{I}} + \mathbb{V}_{45}\bar{\mathbb{R}} + d_4\frac{\partial^2 \bar{\mathbb{I}}}{\partial \mathbb{X}^2}\\
\frac{\partial \bar{\mathbb{R}}}{\partial t} &= \mathbb{V}_{51}\bar{\mathbb{S}} + \mathbb{V}_{52}\bar{\mathbb{E}} + \mathbb{V}_{53}\bar{\mathbb{Q}} + \mathbb{V}_{54}\bar{\mathbb{I}} + \mathbb{V}_{55}\bar{\mathbb{R}} + d_5\frac{\partial^2 \bar{\mathbb{R}}}{\partial \mathbb{X}^2}.
\end{aligned} \tag{4.1}$$

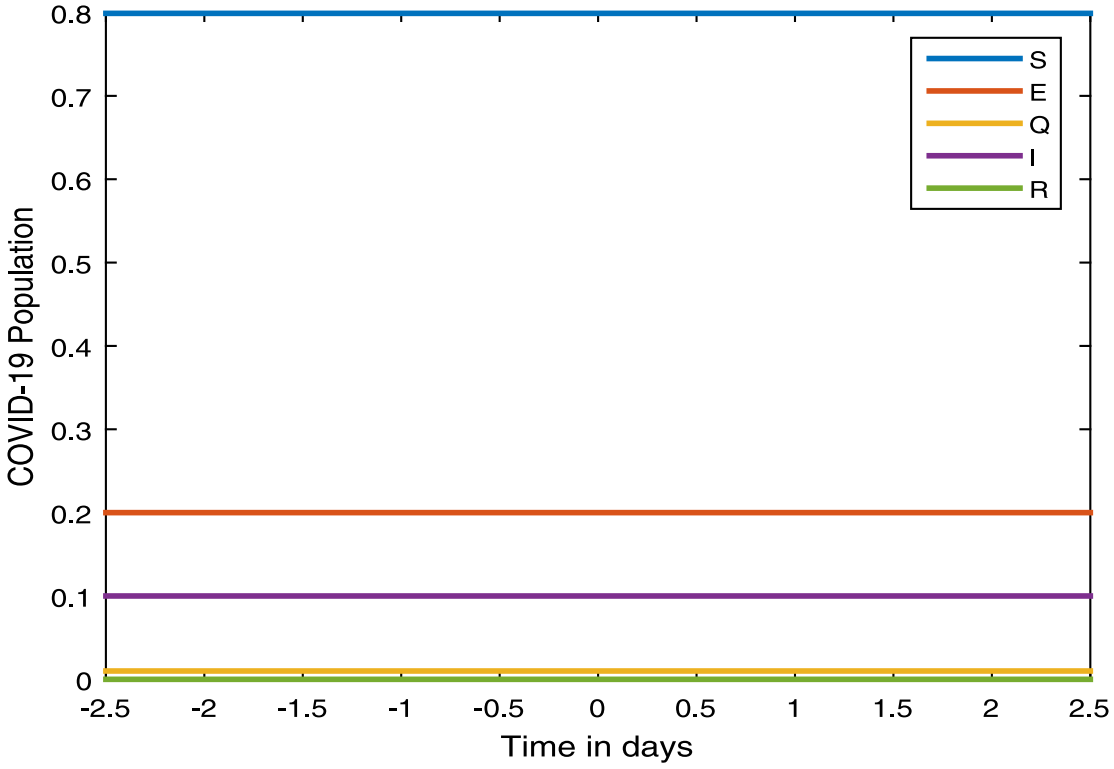

Fig. 2. Profile of the initial condition-1 of the Table 2.

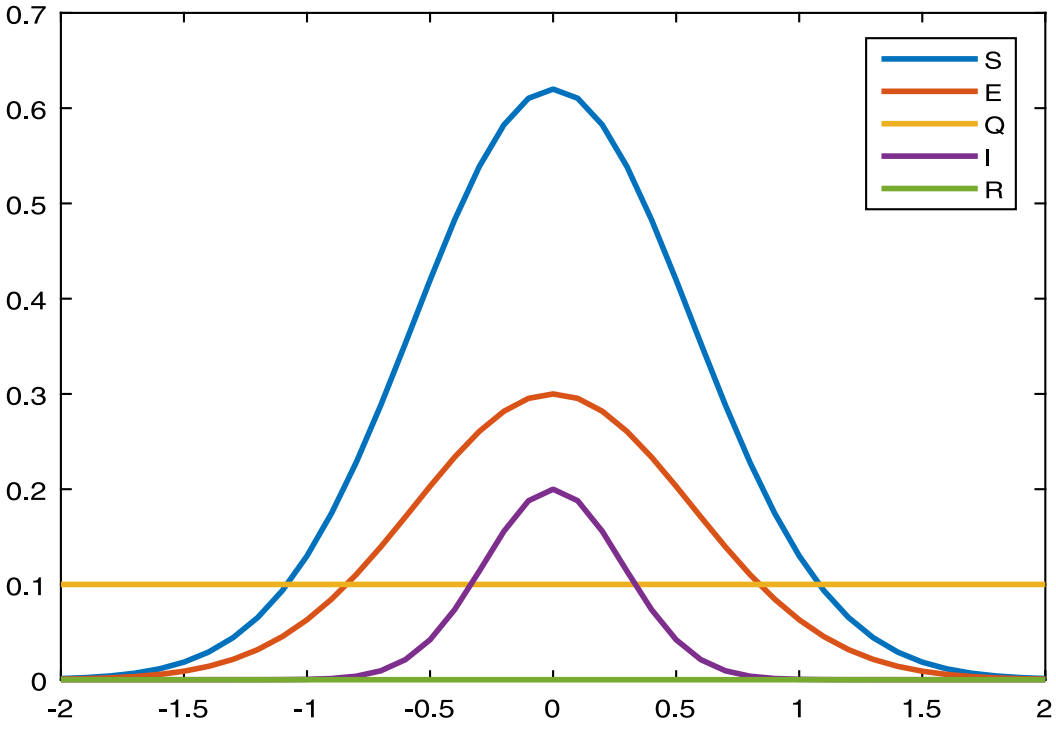

Fig. 3. Profile of the initial condition of the Table 2.

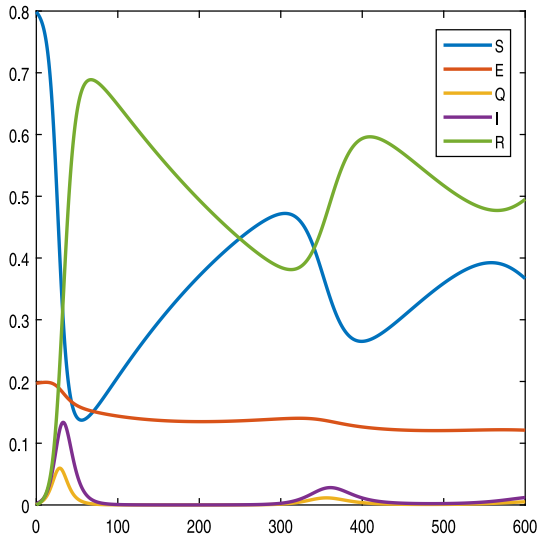

(a) Without diffusion.

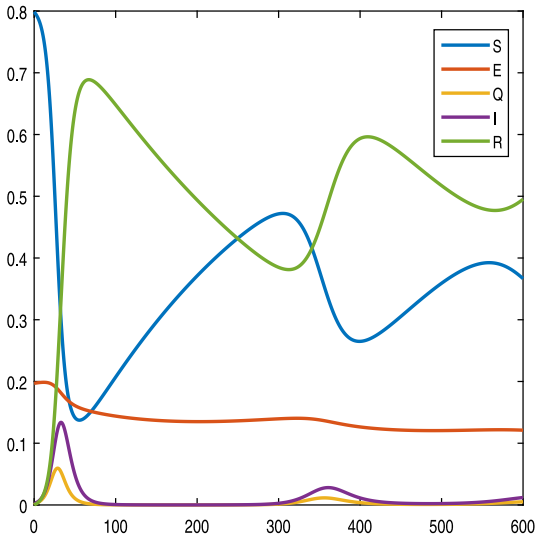

(b) With diffusion.

Fig. 4. Outcomes of the FDOSM for the IC-2 of Table 2, at $\mathbb{X} = 0.0$.

Let the solution of (4.1) be written in Fourier series:

$$\begin{aligned}
\bar{\mathbb{S}}(\mathbb{X},t) &= \sum_k \bar{\mathbb{S}}_k e^{\lambda t}\cos(k\mathbb{X})\\
\bar{\mathbb{E}}(\mathbb{X},t) &= \sum_k \bar{\mathbb{E}}_k e^{\lambda t}\cos(k\mathbb{X})\\
\bar{\mathbb{Q}}(\mathbb{X},t) &= \sum_k \bar{\mathbb{Q}}_k e^{\lambda t}\cos(k\mathbb{X})\\
\bar{\mathbb{I}}(\mathbb{X},t) &= \sum_k \bar{\mathbb{I}}_k e^{\lambda t}\cos(k\mathbb{X})\\
\bar{\mathbb{R}}(\mathbb{X},t) &= \sum_k \bar{\mathbb{R}}_k e^{\lambda t}\cos(k\mathbb{X}).
\end{aligned} \tag{4.2}$$

Where $k = \frac{n\pi}{2}, (n = 1, 2, 3, \ldots)$ and using in Eqs. (4.1) we get

$$\begin{aligned}
&\sum_k \left(\mathbb{V}_{11} - d_1k^2 - \lambda\right)\bar{\mathbb{S}}_k + \sum_k \mathbb{V}_{12}\bar{\mathbb{E}}_k + \sum_k \mathbb{V}_{13}\bar{\mathbb{Q}}_k\\
&\quad + \sum_k \mathbb{V}_{14}\bar{\mathbb{I}}_k + \sum_k \mathbb{V}_{15}\bar{\mathbb{R}}_k = 0\\
&\sum_k \mathbb{V}_{21}\bar{\mathbb{S}}_k + \sum_k \left(\mathbb{V}_{22} - d_2k^2 - \lambda\right)\bar{\mathbb{E}}_k + \sum_k \mathbb{V}_{23}\bar{\mathbb{Q}}_k\\
&\quad + \sum_k \mathbb{V}_{24}\bar{\mathbb{I}}_k + \sum_k \mathbb{V}_{25}\bar{\mathbb{R}}_k = 0\\
&\sum_k \mathbb{V}_{31}\bar{\mathbb{S}}_k + \sum_k \mathbb{V}_{32}\bar{\mathbb{E}}_k + \sum_k \left(\mathbb{V}_{33} - d_3k^2 - \lambda\right)\bar{\mathbb{Q}}_k\\
&\quad + \sum_k \mathbb{V}_{34}\bar{\mathbb{I}}_k + \sum_k \mathbb{V}_{35}\bar{\mathbb{R}}_k = 0\\
&\sum_k \mathbb{V}_{41}\bar{\mathbb{S}}_k + \sum_k \mathbb{V}_{42}\bar{\mathbb{E}}_k + \sum_k \mathbb{V}_{43}\bar{\mathbb{Q}}_k\\
&\quad + \sum_k \left(\mathbb{V}_{44} - d_4k^2 - \lambda\right)\bar{\mathbb{I}}_k + \sum_k \mathbb{V}_{45}\bar{\mathbb{R}}_k = 0\\
&\sum_k \mathbb{V}_{51}\bar{\mathbb{S}}_k + \sum_k \mathbb{V}_{52}\bar{\mathbb{E}}_k + \sum_k \mathbb{V}_{53}\bar{\mathbb{Q}}_k + \sum_k \mathbb{V}_{54}\bar{\mathbb{I}}_k\\
&\quad + \sum_k \left(\mathbb{V}_{55} - d_5k^2 - \lambda\right)\bar{\mathbb{R}}_k = 0.
\end{aligned} \tag{4.3}$$

The Variational matrix V^1 for the system (4.3)

$$V^1 = \begin{bmatrix}
\mathbb{V}_{11} - d_1k^2 & \mathbb{V}_{12} & \mathbb{V}_{13} & \mathbb{V}_{14} & \mathbb{V}_{15}\\
\mathbb{V}_{21} & \mathbb{V}_{22} - d_2k^2 & \mathbb{V}_{23} & \mathbb{V}_{24} & \mathbb{V}_{25}\\
\mathbb{V}_{31} & \mathbb{V}_{32} & \mathbb{V}_{33} - d_3k^2 & \mathbb{V}_{34} & \mathbb{V}_{35}\\
\mathbb{V}_{41} & \mathbb{V}_{42} & \mathbb{V}_{43} & \mathbb{V}_{44} - d_4k^2 & \mathbb{V}_{45}\\
\mathbb{V}_{51} & \mathbb{V}_{52} & \mathbb{V}_{53} & \mathbb{V}_{54} & \mathbb{V}_{55} - d_5k^2
\end{bmatrix}, \tag{4.4}$$

where

$$\begin{cases}
\mathbb{V}_{11} = -\beta\gamma_1\gamma_2\mathbb{E}^* - d \quad \mathbb{V}_{12} = -\beta\gamma_1\gamma_2\mathbb{S}^* \quad \mathbb{V}_{13} = b_1,\\
\quad \mathbb{V}_{14} = 0, \quad \mathbb{V}_{15} = 0,\\
\mathbb{V}_{21} = \beta\gamma_1\gamma_2\mathbb{E}^*, \quad \mathbb{V}_{22} = -\beta\gamma_1\gamma_2\mathbb{S}^* - \left(b_2 + \alpha + \sigma + d\right),\\
\quad \mathbb{V}_{23} = 0, \quad \mathbb{V}_{24} = 0,\\
\mathbb{V}_{31} = 0, \quad \mathbb{V}_{32} = b_2, \quad \mathbb{V}_{33} = -\left(b_1 + c + d\right), \quad \mathbb{V}_{34} = 0,\\
\quad \mathbb{V}_{35} = 0, \quad \mathbb{V}_{25} = 0,\\
\mathbb{V}_{41} = 0 \quad , \mathbb{V}_{42} = \alpha, \quad \mathbb{V}_{43} = c, \quad \mathbb{V}_{44} = -(n + d + \delta), \quad \mathbb{V}_{45} = 0,\\
\mathbb{V}_{51} = 0, \mathbb{V}_{52} = 0, \mathbb{V}_{53} = \sigma, \mathbb{V}_{53} = \eta, \mathbb{V}_{55} = -d.
\end{cases} \tag{4.5}$$

At the endemic equilibrium point E^* the is characteristic equation of the model (2.2) takes the following form:

$$[\lambda + (d_5k^2 + d)][\lambda + (d_4k^2 + \eta + d + \delta)][\lambda^3 + C_1\lambda^2 + C_2\lambda + C_3] = 0, \tag{4.6}$$

where

$$\begin{aligned}
C_1 =& \mathbb{V}_{11} - d_1k^2 + \mathbb{V}_{22} - d_2k^2 + \mathbb{V}_{33} - d_3k^2,\\
C_2 =& \mathbb{V}_{11}\mathbb{V}_{22} - \mathbb{V}_{11}d_2k^2 - \mathbb{V}_{22}d_1k^2 + d_1d_2k^2k^2 + \mathbb{V}_{11}\mathbb{V}_{33}\\
&- \mathbb{V}_{33}d_1k^2 - d_3k^2\mathbb{V}_{11} + d_1d_3k^2k^2\\
&+ \mathbb{V}_{22}\mathbb{V}_{33} - \mathbb{V}_{22}d_3k^2 - \mathbb{V}_{33}d_2k^2 + d_2d_3k^2k^2 - \mathbb{V}_{12}\mathbb{V}_{21},\\
C_3 =& -\mathbb{V}_{11}\mathbb{V}_{22}\mathbb{V}_{33} + \mathbb{V}_{11}\mathbb{V}_{33}d_2k^2 + \mathbb{V}_{22}\mathbb{V}_{33}d_1k^2\\
&- \mathbb{V}_{33}d_1d_2k^2k^2 + \mathbb{V}_{11}\mathbb{V}_{22}d_3k^2 - \mathbb{V}_{11}d_2k^2d_3k^2\\
&- \mathbb{V}_{22}d_1k^2 + d_1d_2d_3k^2k^2k^2.
\end{aligned} \tag{4.7}$$

The Routh–Hurwitz criterion[36] for stability gives $C_i > 0, i = 1, 2, 3$ and $C_1C_2 - C_3 > 0$.

5. Discretization space and time

In the present section, we utilize MEM, FDOSM and MOSM for the numerical solutions of the system (2.2). In all cases, time step $\Delta t = 0.024$ days and spatial step $\Delta\mathbb{X} = 0.1$ are used.

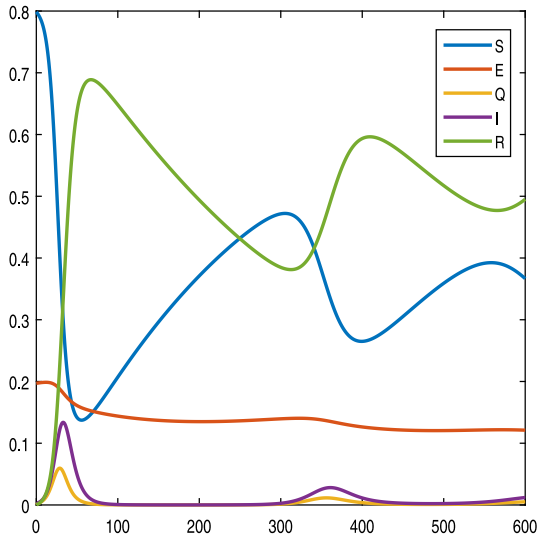

(a) With diffusion.

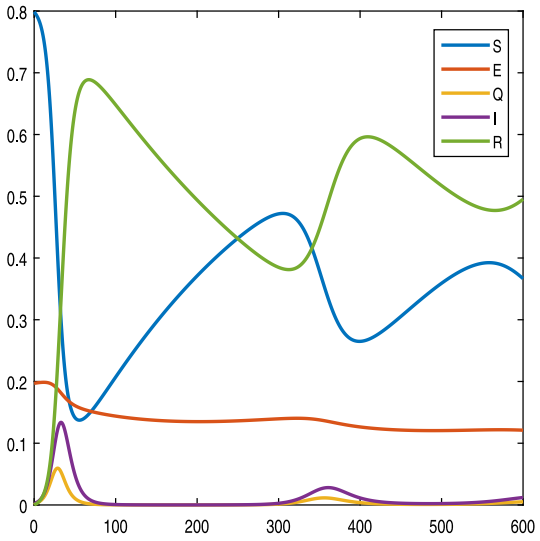

(b) With diffusion.

Fig. 5. Outcomes of the MOSM (L) and the MEM (R) for the IC-1 of Table 2, at $\mathbb{X} = 0.0$.

Table 2
Initial condition.

Symbols	Initial condition-1	Initial condition-1	Domain
$\mathbb{S}$	0.799	$0.71\exp\left(-(\mathbb{X}/1.4)^2\right)$	$\mathbb{X}\in[-2.5,2.5]$
$\mathbb{E}$	0.2	$0.41\exp\left(-(\mathbb{X}/1.4)^2\right)$	$\mathbb{X}\in[-2.5,2.5]$
$\mathbb{Q}$	0.01	0.3	$\mathbb{X}\in[-2.5,2.5]$
$\mathbb{I}$	0.2	$0.25\exp\left(-\mathbb{X}^2\right)$	$\mathbb{X}\in[-2.5,2.5]$
$\mathbb{R}$	0.0	0.0	$\mathbb{X}\in[-2.5,2.5]$

5.1. Explicit discretization of time based on forward difference operator

Forward difference approximation of the first-order is applied on the system (2.2) gives us:

$$\begin{aligned}
\frac{\mathbb{S}^{n+1}-\mathbb{S}^n}{dt} &= A-\beta\gamma_1\gamma_2\mathbb{S}^n\mathbb{E}^n+b_1\mathbb{Q}^n-dS^n+d_1\frac{\partial^2\mathbb{S}^n}{\partial\mathbb{X}^2}\\
\frac{\mathbb{E}^{n+1}-\mathbb{E}^n}{dt} &= \beta\gamma_1\gamma_2\mathbb{S}^n\mathbb{E}^n-b_2\mathbb{E}^n-\alpha\mathbb{E}^n-\sigma\mathbb{E}^n-d\mathbb{E}^n+d_2\frac{\partial^2\mathbb{E}^n}{\partial\mathbb{X}^2}\\
\frac{\mathbb{Q}^{n+1}-\mathbb{Q}^n}{dt} &= b_2\mathbb{E}^n-b_1\mathbb{Q}^n-cQ^n-d\mathbb{Q}^n+d_3\frac{\partial^2\mathbb{Q}^n}{\partial\mathbb{X}^2}\\
\frac{\mathbb{I}^{n+1}-\mathbb{I}^n}{dt} &= \alpha\mathbb{E}^n+c\mathbb{Q}^n-(\eta+d+\delta)\mathbb{I}^n+d_4\frac{\partial^2\mathbb{I}^n}{\partial\mathbb{X}^2}\\
\frac{\mathbb{R}^{n+1}-\mathbb{R}^n}{dt} &= \eta\mathbb{I}^n+\sigma\mathbb{E}^n-d\mathbb{R}^n+d_5\frac{\partial^2\mathbb{R}^n}{\partial\mathbb{X}^2}.
\end{aligned} \tag{5.1}$$

5.2. Discretization of time based on operator splitting

The discretization is carried out in two phase. In the first phase the first-order time difference is discretized by considering the half time step from t^n to t^n+dt^* as:

$$\begin{aligned}
\frac{\mathbb{S}^{n+\frac{1}{2}}-\mathbb{S}^n}{dt^*} &= A-\beta\gamma_1\gamma_2\mathbb{S}^n\mathbb{E}^n+b_1\mathbb{Q}^n-d\mathbb{S}^n\\
\frac{\mathbb{E}^{n+\frac{1}{2}}-\mathbb{S}^n}{dt^*} &= \beta\gamma_1\gamma_2\mathbb{S}^n\mathbb{E}^n-b_2\mathbb{E}^n-\alpha\mathbb{E}^n-\sigma\mathbb{E}^n-d\mathbb{E}^n\\
\frac{\mathbb{Q}^{n+\frac{1}{2}}-\mathbb{Q}^n}{dt^*} &= b_2\mathbb{E}^n-b_1\mathbb{Q}^n-c\mathbb{Q}^n-d\mathbb{Q}^n\\
\frac{\mathbb{I}^{n+\frac{1}{2}}-\mathbb{I}^n}{dt^*} &= \alpha\mathbb{E}^n+c\mathbb{Q}^n-(\eta+d+\delta)\mathbb{I}^n\\
\frac{\mathbb{R}^{n+\frac{1}{2}}-\mathbb{R}^n}{dt^*} &= \eta\mathbb{I}^n+\sigma\mathbb{E}^n-d\mathbb{R}^n.
\end{aligned} \tag{5.2}$$

From t^n+dt^* to t^{n+1} in the 2nd step

$$\begin{aligned}
\frac{\mathbb{S}^{n+1}-\mathbb{S}^{n+\frac{1}{2}}}{dt^*} &= d_1\frac{\partial^2\mathbb{S}^{n+\frac{1}{2}}}{\partial\mathbb{X}^2},\\
\frac{\mathbb{E}^{n+1}-\mathbb{E}^{n+\frac{1}{2}}}{dt^*} &= d_2\frac{\partial^2\mathbb{E}^{n+\frac{1}{2}}}{\partial\mathbb{X}^2},\\
\frac{\mathbb{Q}^{n+1}-\mathbb{Q}^{n+\frac{1}{2}}}{dt^*} &= d_3\frac{\partial^2\mathbb{Q}^{n+\frac{1}{2}}}{\partial\mathbb{X}^2},\\
\frac{\mathbb{I}^{n+1}-\mathbb{I}^{n+\frac{1}{2}}}{dt^*} &= d_4\frac{\partial^2\mathbb{I}^{n+\frac{1}{2}}}{\partial\mathbb{X}^2},\\
\frac{\mathbb{R}^{n+1}-\mathbb{R}^{n+\frac{1}{2}}}{dt^*} &= d_5\frac{\partial^2\mathbb{R}^{n+\frac{1}{2}}}{\partial\mathbb{X}^2},
\end{aligned} \tag{5.3}$$

where $dt^*=\frac{dt}{2}$.

5.3. Discretization of space based on MQ RBF

In second-order finite difference scheme Eq. (5.3) is:

$$\frac{\partial^2\eta^{*n+\frac{1}{2}}}{\partial\mathbb{X}^2}=\frac{\eta_{i-1}^{*n+\frac{1}{2}}+2\eta_i^{*n+\frac{1}{2}}+\eta_{i+1}^{*n+\frac{1}{2}}}{\Delta\mathbb{X}^2}, \tag{5.4}$$

where the symbol $\eta^*=\mathbb{S},\mathbb{E},\mathbb{Q},\mathbb{I},\mathbb{R}$. Considering N centers, $\zeta_1,\zeta_2,\dots,\zeta_N,\in R^d$, we have

$$P(\zeta)=\sum_{j=1}^{N}\alpha_j\psi\left(\left\|\zeta-\zeta_j\right\|_2\right)=\sum_{j=1}^{N}\alpha_j\psi(r),\quad \zeta\in R^d. \tag{5.5}$$

Where $\psi(r)$ is radial basis function (RBF) and $r=\sqrt{(\zeta_i-\zeta_k)^2}, i,k=1,2,\dots,N$. Here we obtained $\alpha_i, j=1,\dots,N$ from

$$P\left(\zeta_i\right)=\mathcal{F}_i,\quad i=1,2,\dots,M \tag{5.6}$$

at a set of nodal points $\zeta_i, i=1,2,\dots,M$. As centers and collocation points are same. Hence

$$\mathbf{B}\alpha=\mathbf{f}. \tag{5.7}$$

Where $\mathbf{B}$ is an $N\times N$ interpolation matrix and the coefficients $\alpha_j, j=1,\dots,N$ is $N\times 1$, having the following entries;

$$\mathbf{B}=(\psi)_{ij}=\psi\left\|\zeta_i-\zeta_j\right\|_2=\sqrt{(\zeta_i-\zeta_j)^2+c^2},\quad i,j=1,2,\dots,N \tag{5.8}$$

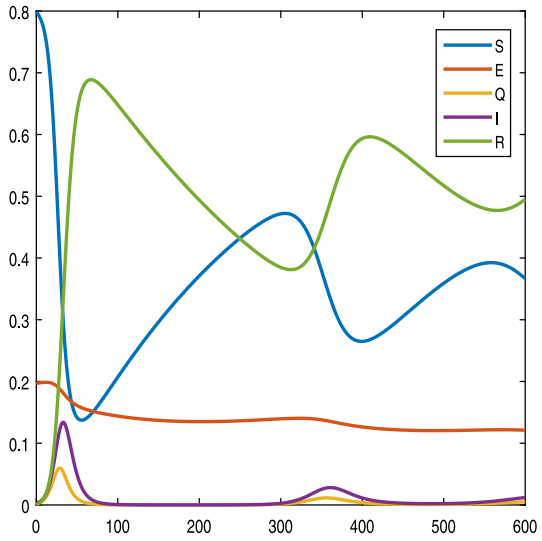

(a) Without diffusion.

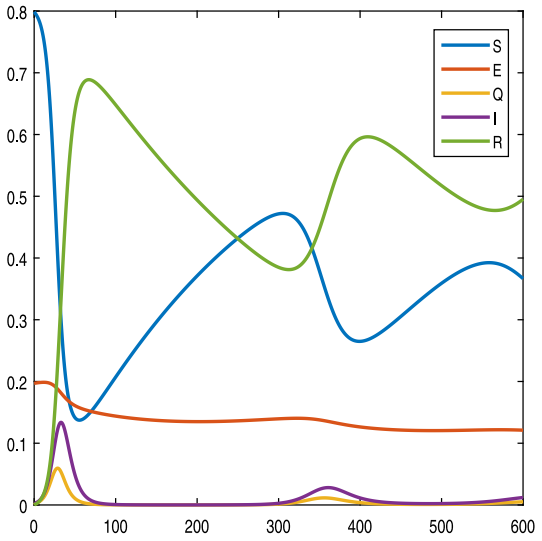

(b) With diffusion.

Fig. 6. Outcomes of the FDOSM for the IC-1 of Table 2, at $\mathbb{X} = 0.0$.

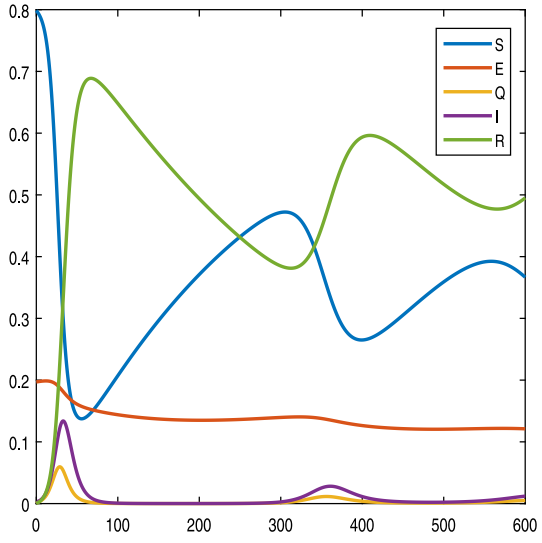

(a) With diffusion.

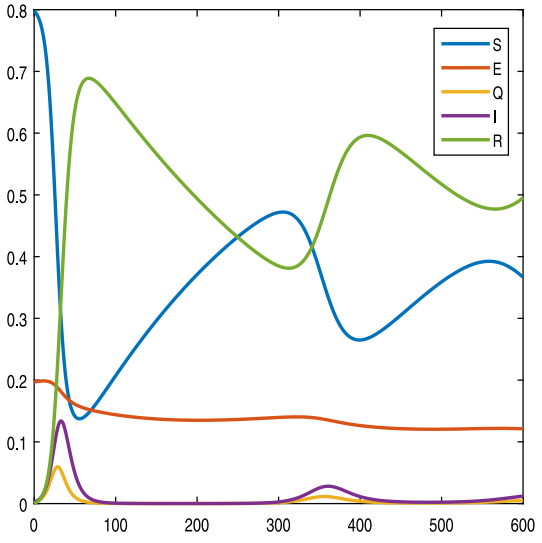

(b) With diffusion.

Fig. 7. Outcomes of the MOSM (L) and the MEM (R) for the IC-1 of Table 2, at $\mathbb{X} = 1.0$.

where

$$\mathbf{B} = \begin{bmatrix} \psi\left(\|\zeta_1 - \zeta_1\|_2\right) & \psi\left(\|\zeta_1 - \zeta_2\|_2\right) & \cdots & \psi\left(\|\zeta_1 - \zeta_N\|_2\right) \\ \psi\left(\|\zeta_2 - \zeta_1\|_2\right) & \psi\left(\|\zeta_2 - \zeta_2\|_2\right) & \cdots & \psi\left(\|\zeta_2 - \zeta_N\|_2\right) \\ \vdots & \vdots & \vdots & \vdots \\ \psi\left(\|\zeta_N - \zeta_1\|_2\right) & \psi\left(\|\zeta_N - \zeta_2\|_2\right) & \cdots & \psi\left(\|\zeta_N - \zeta_N\|_2\right) \end{bmatrix} \tag{5.9}$$

and

$$\mathbf{f} = \left[\mathcal{F}_1, \mathcal{F}_2, \ldots, \mathcal{F}_N\right]^t. \tag{5.10}$$

The MQ RBF method is currently applied to track down the graphical outcomes of the model (2.2) which is known as the meshless strategy. The RBFs estimate for the derivatives of $f(\boldsymbol{\zeta})$ can be addressed by

$$\mathcal{D}P(\boldsymbol{\zeta}) = \sum_{k=1}^{N} \mathcal{D}\psi(\mathbf{r})\alpha_k = \mathbf{B}_{\mathrm{d}}\alpha \tag{5.11}$$

where

$$\mathbf{B_d} = \begin{bmatrix} \mathcal{D}\psi\left(\|\zeta_1 - \zeta_1\|_2\right) & \mathcal{D}\psi\left(\|\zeta_1 - \zeta_2\|_2\right) & \cdots & \mathcal{D}\psi\left(\|\zeta_1 - \zeta_N\|_2\right) \\ \mathcal{D}\psi\left(\|\zeta_2 - \zeta_1\|_2\right) & \mathcal{D}\psi\left(\|\zeta_2 - \zeta_2\|_2\right) & \cdots & \mathcal{D}\psi\left(\|\zeta_2 - \zeta_N\|_2\right) \\ \vdots & \vdots & \vdots & \vdots \\ \mathcal{D}\psi\left(\|\zeta_N - \zeta_1\|_2\right) & \mathcal{D}\psi\left(\|\zeta_N - \zeta_2\|_2\right) & \cdots & \mathcal{D}\psi\left(\|\zeta_N - \zeta_N\|_2\right) \end{bmatrix}. \tag{5.12}$$

Here $\mathcal{D}$ is like this;

$$\begin{aligned} \mathcal{D}(*) &= \frac{\partial^2 *}{\partial \zeta^2} \quad \text{if } *\in \Omega \\ \mathcal{D}(*) &= \frac{\partial *}{\partial \zeta} \quad \text{if } *\in \partial\Omega, \end{aligned} \tag{5.13}$$

hence the system (2.2) can be written as;

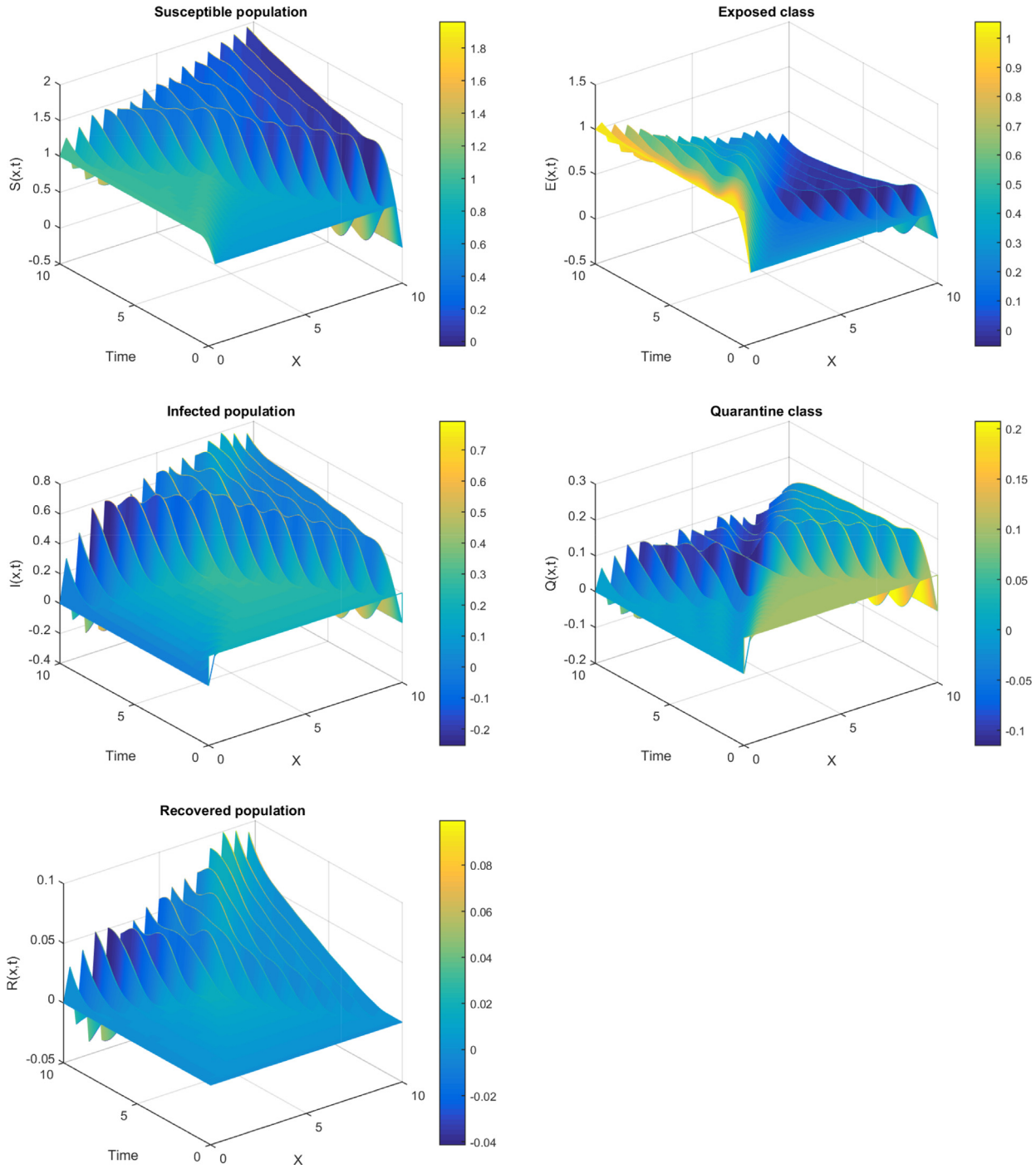

Fig. 8. Profiles for the first set of initial conditions of Table 2 by FDOSM method.

Step 1

From 0 to dt^*

$$\begin{aligned}
\mathbb{S}^{n+\frac{1}{2}} &= \mathbb{S}^n + dt^*[A - \beta\gamma_1\gamma_2\mathbb{S}^n\mathbb{E}^n + b_1\mathbb{Q}^n - d\mathbb{S}^n]\\
\mathbb{E}^{n+\frac{1}{2}} &= \mathbb{E}^n + dt^*[\beta\gamma_1\gamma_2\mathbb{S}^n\mathbb{E}^n - b_2\mathbb{E}^n - \alpha\mathbb{E}^n - \sigma\mathbb{E}^n - d\mathbb{E}^n]\\
\mathbb{Q}^{n+\frac{1}{2}} &= \mathbb{Q}^n + dt^*[b_2\mathbb{E}^n - b_1\mathbb{Q}^n - c\mathbb{Q}^n - d\mathbb{Q}^n]\\
\mathbb{I}^{n+\frac{1}{2}} &= \mathbb{I}^n + dt^*[\alpha\mathbb{E}^n + c\mathbb{Q}^n - (\eta + d + \delta)\mathbb{I}^n]\\
\mathbb{R}^{n+\frac{1}{2}} &= \mathbb{R}^n + dt^*[\eta\mathbb{I}^n + \sigma\mathbb{E}^n - d\mathbb{R}^n].
\end{aligned} \tag{5.14}$$

Step 2

From dt^* to dt

$$\mathbf{B_d}\alpha^{n+\frac{1}{2}} = \mathbf{F}. \tag{5.15}$$

$$\mathbf{F}(\zeta) = \left[f\left(\zeta_1\right), f\left(\zeta_2\right), \ldots, f\left(\zeta_N\right)\right]^t. \tag{5.16}$$

$$\alpha^{n+\frac{1}{2}} = \left[\alpha_1^{n+\frac{1}{2}}, \alpha_2^{n+\frac{1}{2}}, \ldots, \alpha_N^{n+\frac{1}{2}}\right]^t. \tag{5.17}$$

Here

$$\mathcal{F}_i = \eta^{*n+\frac{1}{2}}dt + d_j^*\frac{\partial^2\eta^{*n+\frac{1}{2}}}{\partial\zeta^2} \quad j = 1, \ldots, 5, \quad i = 1, 2, \ldots, N \tag{5.18}$$

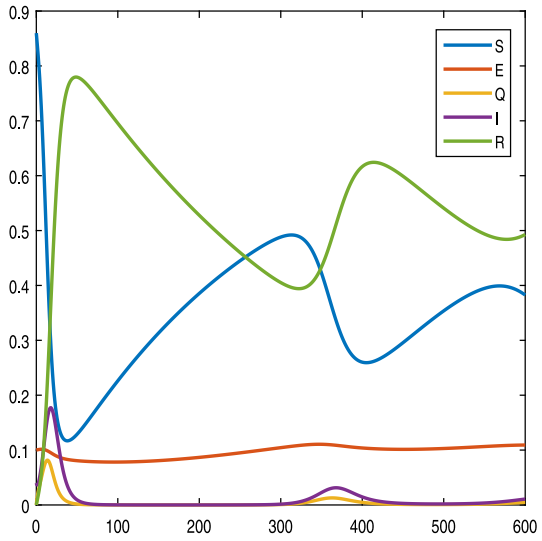

(a) Without diffusion.

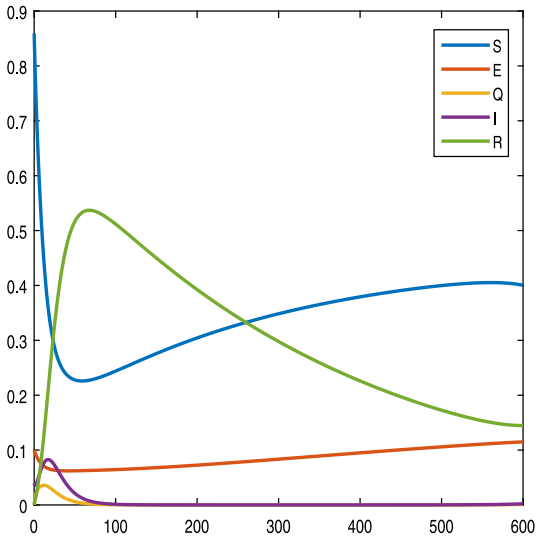

(b) With diffusion.

Fig. 9. Outcomes of the FDOSM for the IC-2 of Table 2, at $\mathbb{X} = 0.0$.

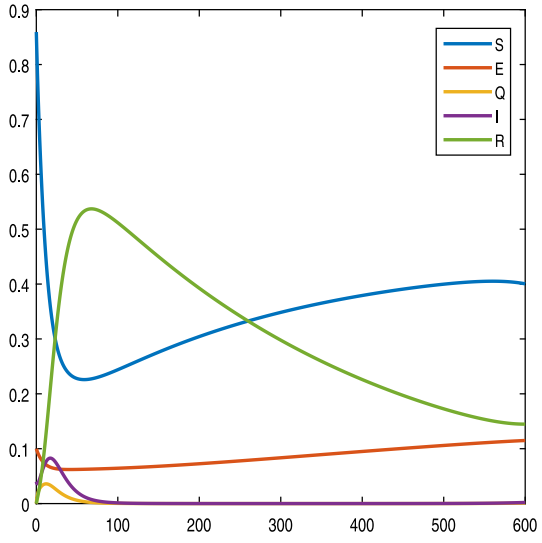

(a) With diffusion.

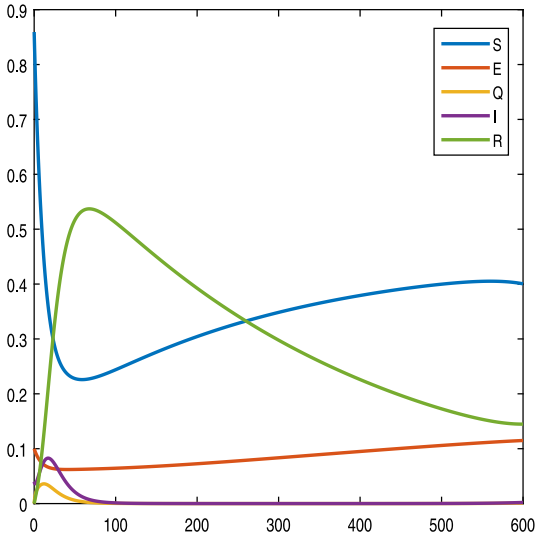

(b) With diffusion.

Fig. 10. Outcomes of the MOSM (L) and the MEM (R) for the IC-2 of Table 2, at $\mathbb{X} = 0.0$.

where $\eta^* = \mathbb{S}, \mathbb{E}, \mathbb{Q}, \mathbb{I}, \mathbb{R}$

$$\eta^{*n+\frac{1}{2}} = \sum_{j=1}^{N} \alpha_j^{n+\frac{1}{2}} \psi\left(\left\|\zeta - \zeta_j^c\right\|_2\right), \quad \zeta \in R. \tag{5.19}$$

$$\frac{\partial^2 \eta^{*n+\frac{1}{2}}}{\partial \zeta^2} = \sum_{j=1}^{N} \alpha_j^{n+\frac{1}{2}} \frac{\partial^2 \psi\left(\left\|\zeta - \zeta_j^c\right\|_2\right)}{\partial \zeta^2}, \tag{5.20}$$

where

$$\mathbf{B_d} = \left(b_{sk}\right) = \mathcal{L}\psi\left(\left\|\zeta_s - \zeta_k\right\|\right), \quad s, k = 1, 2, \ldots, N \tag{5.21}$$

is the skth matrix element of the $N \times N$ matrix $\mathbf{B_d}$. The coefficients $\alpha_k^{n+\frac{1}{2}}, k = 1, 2, \ldots, N$ can be found using the Eq. (5.15). The Gauss Elimination or LU-factorization technique can be utilize for the solution the system (5.15).

6. Parameter estimation

Here we utilized the least square curve fitting for the recorded COVID-19 cases in Pakistan from 04 March to May 10, 2020. The estimated values of the parameters are shown in Table 1.

7. Initial conditions

The following sets of initial conditions are utilized in the numerical outcomes to check the effectiveness of the proposed numerical techniques (see Figs. 1–3).

8. Numerical simulations

We consider the initial condition in Table 2. For the numerical solution of (2.2), the parameters values given in Table 1 are considered.

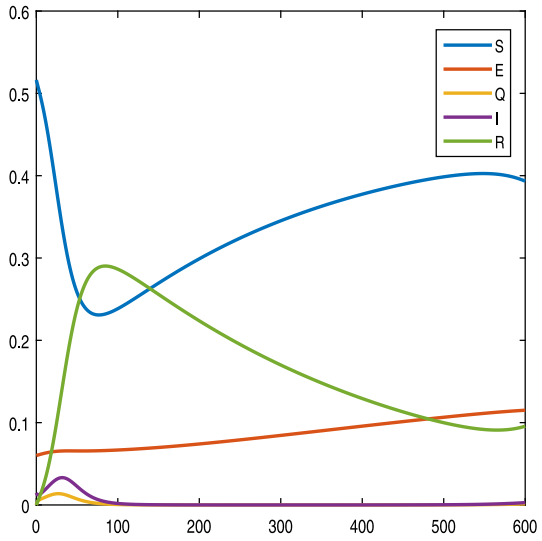

(a) Without diffusion.

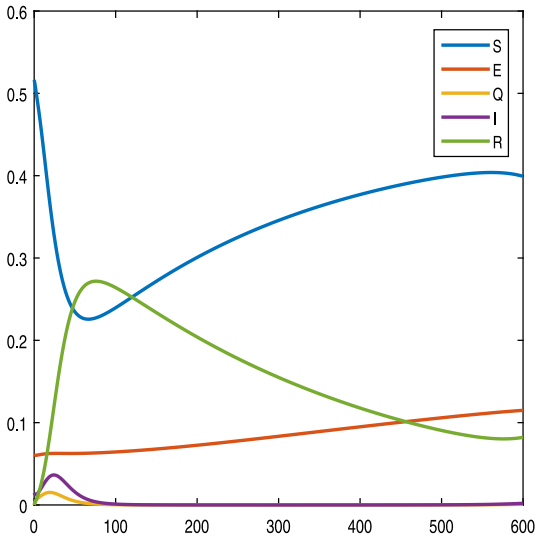

(b) With diffusion.

Fig. 11. Outcomes of the FDOSM for the IC-2 of Table 2, at $\mathbb{X} = 0.0$.

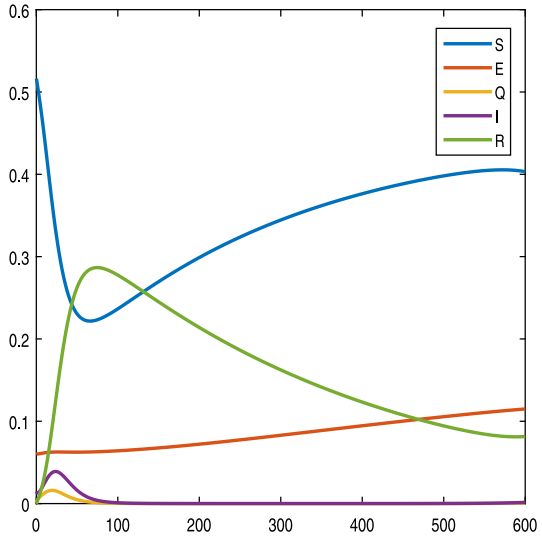

(a) With diffusion.

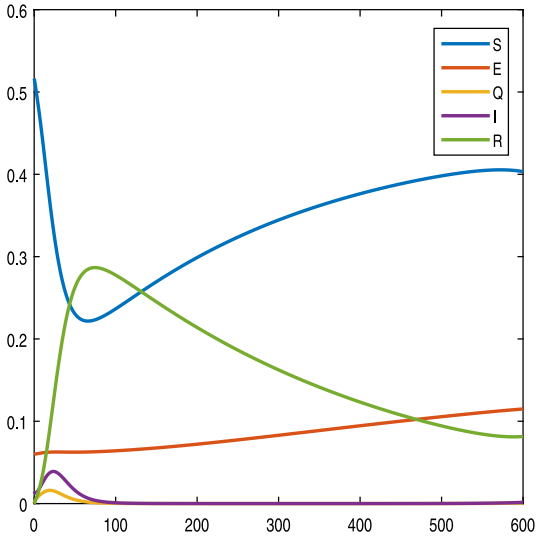

(b) With diffusion.

Fig. 12. Outcomes of the MOSM (L) and the MEM (R) for the IC-2 of Table 2, at $\mathbb{X} = 1.0$.

Analysis are conducted at certain points within the domain, i.e., $\mathbb{X} = 0.0$ and $\mathbb{X} = 1.0$ for 600 days. By using meshless methods, this study had the added advantage that the results were extended to nonlinear PDEs based on RBF algorithms. Compared with other approaches, this one can work on data scattered over a set of nodes without requiring underlying meshes. The meshless methods also have the advantage of being able to be extended to high-dimensional reaction diffusion models. In this experiment, ultimately, we wish to determine whether meshless epidemiological models are capable and competitive with state-of-the-art methods for large-scale epidemiological modeling. Our simulated results are based on the shape parameter $C = \frac{100}{N}$.

8.1. *Initial condition-1 of Table 2 at* $\mathbb{X} = 0.0$

Fig. 4 shows the results from the simulation of the FDOSM with and without diffusion with the initial condition 1 from Table 2. Neither the model with nor without diffusion produces a significant difference in output. MEM and MOSM computations along with the same initial conditions are depicted in Fig. 5. Accordingly, the FDOSM and MOSM yield numerical results which are similar across populations. Compared to its counterpart FDOSM, the simulated results obtained through FDOSM and MOSM of the class R are a little smaller.

8.2. *Initial condition-1 of Table 2 at* $\mathbb{X} = 1.0$

See Figs. 6–8.

8.3. *Initial condition-2 of Table 2 at* $\mathbb{X} = 0.0$

Fig. 9 shows the results from the simulation of the FDOSM with and without diffusion with the initial condition 1 from Table 2. MEM and MOSM computations along with the same initial conditions are

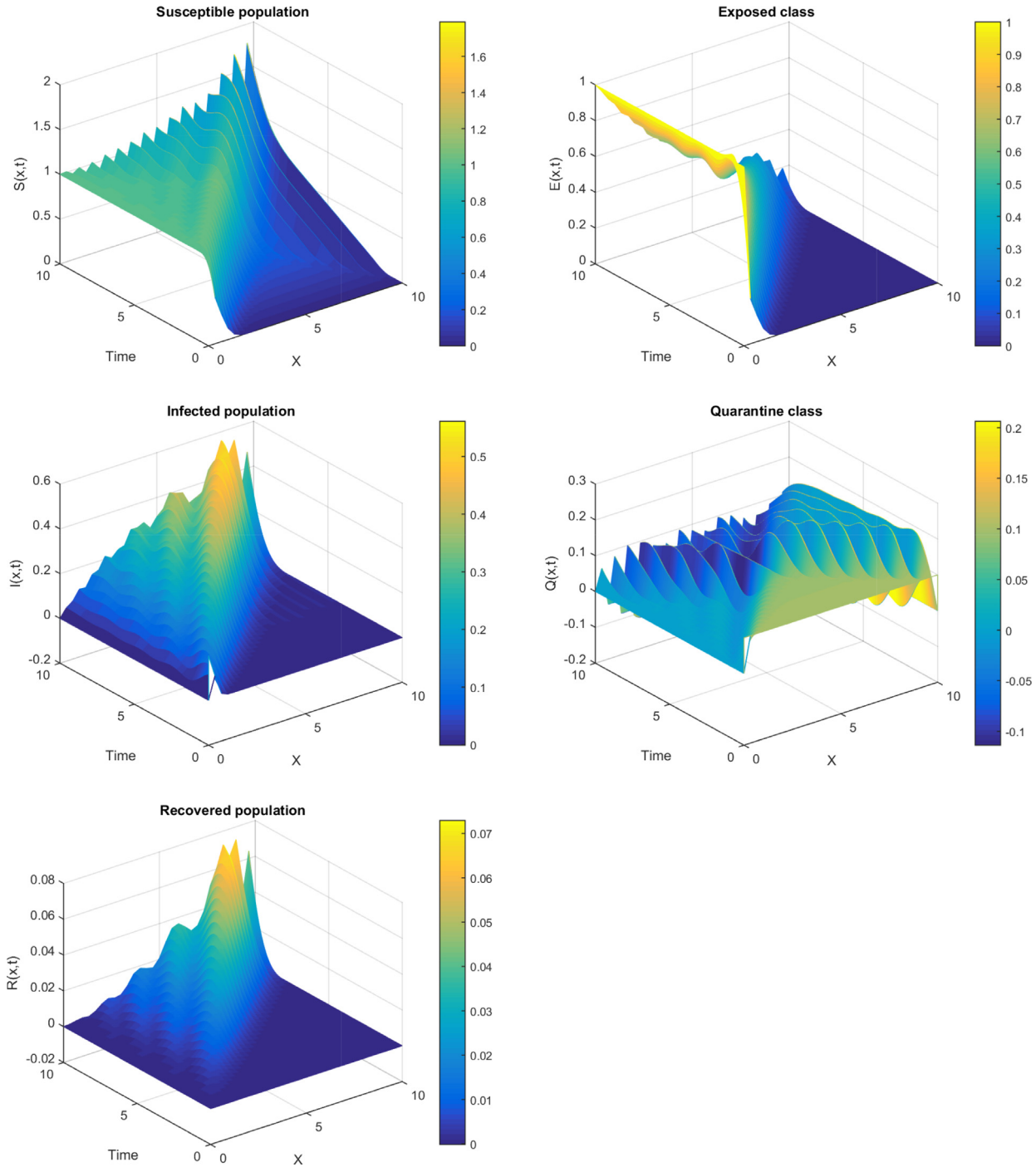

Fig. 13. Profiles for the second set of initial conditions of Table 2 by FDOSM method.

depicted in Fig. 10. It is clear from the figures that the graph of class S round about at $t = 70$ days is higher in the system having diffusion. This is due to the mobility of population reduced the chances of susceptible class to be exposed and which leads to the downfall in the graphs of the classes $\mathbb{I}$ and $\mathbb{R}$ in the event of diffusion.

8.4. *Initial condition of Table 2 at* $\mathbb{X} = 1.0$

With the IC-2 of Table 2 the results produced by FDOSM without and with diffusion are indicated in Fig. 11. While the graphical Outcomes along with the same initial condition produced by MEM and MOSM are shown in Fig. 12. In this case, the population at $\mathbb{X} = 1.0$ is smaller is compared to the previous case at $\mathbb{X} = 0.0$.

9. Conclusions

This paper presents a new mathematical model for capturing the spread of diseases in moving individuals using partial differential equations. To simulate the epidemiological compartmental model with high non-linearity $SEQIR$, three methods for the numerical solution have been proposed and compared. Furthermore, the diffusion process does not have much impact on the final simulation results of the three methods subject to a uniformly distributed and constant initial population. Diffusion has a more visible effect when the population is normally distributed. This happens because most junk within the population is gathered towards the mean position, and so diffusion facilitates the mixing of groups. In the future, the proposed model can be extended

to a fractional order system by using fractional derivatives or integration like Caputo, Hilfer, Atangana, etc. Further control parameters can be added to the proposed model by using optimal control theory to minimize the infection among the infected individuals. In this regard, suitable optimal control variables along with Hamiltonian and Lagrangian need to be defined (see Fig. 13).

CRediT authorship contribution statement

Rahat Zarin: Conceptualization, Data curation, Validation, Writing – original draft.

Declaration of competing interest

The authors declare that they have no known competing financial interests or personal relationships that could have appeared to influence the work reported in this paper.

Data availability

The authors do not have permission to share data.

Acknowledgments

The author is grateful to the handling editor and reviewers for their constructive comments and remarks which helped to improve the quality of the manuscript.

References

1. Habibzadeh P, Stoneman EK. The novel coronavirus: a bird's eye view. *Int J Occup Med Environ Health*. 2020;11(2):65.
2. Tay MZ, Poh CM, Rénia L, MacAry PA, Ng LF. The trinity of COVID-19: immunity, inflammation and intervention. *Nat Rev Immunol*. 2020;20(6):363–374.
3. Ahmed A, Salam B, Mohammad M, Akgul A, Khoshnaw SH. Analysis coronavirus disease (COVID-19) model using numerical approaches and logistic model. *Aims Bioeng*. 2020;7(3):130–146.
4. Hussain G, Khan T, Khan A, et al. Modeling the dynamics of novel coronavirus (COVID-19) via stochastic epidemic model. *Alex Eng J*. 2021;60(4):4121–4130.
5. Zarin R, Khan A, Kumar P. Fractional-order dynamics of Chagas-HIV epidemic model with different fractional operators. *AIMS Math*. 2022;7(10):18897–18924.
6. Zarin R, Khan A, Akgül A, Akgül EK. Fractional modeling of COVID-19 pandemic model with real data from Pakistan under the ABC operator. *AIMS Math*. 2022;7(9):15939–15964.
7. Aslam M, Farman M, Akgül A, Ahmad A, Sun M. Generalized form of fractional order COVID-19 model with Mittag–Leffler kernel. *Math Methods Appl Sci*. 2021;44(11):8598–8614.
8. Shah K, Abdeljawad T, Mahariq I, Jarad F. Qualitative analysis of a mathematical model in the time of COVID-19. *Biomed Res Int*. 2020;2020(1):1–11.
9. Tong ZW, Lv YP, Din RU, Mahariq I, Rahmat G. Global transmission dynamic of SIR model in the time of SARS-CoV-2. *Results Phys*. 2021;25:104253.
10. Jitsinchayakul S, Zarin R, Khan A, Yusuf A, Zaman G, Sulaiman TA. Fractional modeling of COVID-19 epidemic model with harmonic mean type incidence rate. *Open Phys*. 2021;19(1):693–709.
11. Backer JA, Klinkenberg D, Wallinga J. Incubation period of 2019 novel coronavirus (2019-nCoV) infections among travellers from wuhan, china. *Euro Surveill*. 2020;25(5):2000062.
12. Kronbichler A, Kresse D, Yoon S, Lee KH, Effenberger M, Shin JI. Asymptomatic patients as a source of COVID-19 infections: A systematic review and meta-analysis. *Int J Infect Dis*. 2020;98:180–186.
13. Zarin R, Khan A, Yusuf A, Abdel-Khalek S, Inc M. Analysis of fractional COVID-19 epidemic model under Caputo operator. *Math Methods Appl Sci*. 2021;6(2):115–122.
14. Dal-Ré R, Banzi R, Georgin-Lavialle S, et al. Remdesivir for COVID-19 in Europe: will it provide value for money? *Lancet Respir Med*. 2021;9(2):127–128.
15. Ambikapathy B, Krishnamurthy K. Mathematical modelling to assess the impact of lockdown on COVID-19 transmission in India: model development and validation. *J Med Internet Res*. 2020;6(2):e19368.
16. Khan A, Zarin R, Hussain G, Ahmad NA, Mohd MH, Yusuf A. Stability analysis and optimal control of covid-19 with convex incidence rate in Khyber Pakhtunkhawa (Pakistan). *Results Phys*. 2021;20(2):103703.
17. Khan A, Zarin R, Akgül A, Saeed A, Gul T. Fractional optimal control of COVID-19 pandemic model with generalized Mittag-Leffler function. *Adv Differ Equ*. 2021;(1):1–22.
18. Alqarni MS, Alghamdi M, Muhammad T, Alshomrani AS, Khan MA. Mathematical modeling for novel coronavirus (COVID-19) and control. *Numer Methods Partial Differ Equ*. 2020;21(2):217.
19. Khan A, Zarin R, Khan S, Saeed A, Gul T, Humphries UW. Fractional dynamics and stability analysis of COVID-19 pandemic model under the harmonic mean type incidence rate. *Comput Methods Biomech Biomed Eng*. 2021;8(2):1–22.
20. Li Q, Guan X, Wu P, et al. Early transmission dynamics in Wuhan, China, of novel coronavirus–infected pneumonia. *N Engl J Med*. 2020;8(4):24–37.
21. Yu WB, Tang GD, Zhang L, Corlett RT. Decoding the evolution and transmissions of the novel pneumonia coronavirus (SARS-CoV-2/HCoV-19) using whole genomic data. *Zool Res*. 2020;41(3):247.
22. Kramer A, Schwebke I, Kampf G. How long do nosocomial pathogens persist on inanimate surfaces? A systematic review. *BMC Infect Dis*. 2006;6:130.
23. Fasshauer GE. Meshfree approximation methods with MATLAB. *World Sci*. 2007;(6):1–520.
24. Mai-Duy N, Tran-Cong T. Mesh-free radial basis function network methods with domain decomposition for approximation of functions and numerical solution of Poisson's equations. *Eng Anal Bound Elem*. 2002;26(2):133–156.
25. Ahmad I, Hussain SI, Usman M, Ilyas H. On the solution of Zabolotskaya–Khokhlov and Diffusion of Oxygen equations using a sinc collocation method. *Partial Differ Equ Appl Math*. 2021;4:100066.
26. Golberg MA, Chen CS. The method of fundamental solutions for potential, Helmholtz and diffusion problems. *BIM Numer Math*. 1998;1:103–176.
27. Kansa EJ. Multiquadrics-A scattered data approximation scheme with applications to computational fluid-dynamics—II solutions to parabolic, hyperbolic and elliptic partial differential equations. *Comput Math Appl*. 1990;19(8–9):147–161.
28. Madych WR, Nelson SA. Multivariate interpolation and conditionally positive definite functions. II. *Math Comp*. 1990;54(189):211–230.
29. Micchelli CA. Interpolation of scattered data: distance matrices and conditionally positive definite functions. *Constr Approx*. 1986;2(1):11–22.
30. Prasannakumara BC. Numerical simulation of heat transport in Maxwell nanofluid flow over stretching sheet considering magnetic dipole effect. *Partial Differ Equ Appl Math*. 2021;4:100064.
31. Šarler B, Vertnik R. Meshfree explicit local radial basis function collocation method for diffusion problems. *Comput Math Appl*. 2006;51:1269–1282.
32. Mahariq I, Giden IH, Kurt H, Minin OV, Minin IV. Strong electromagnetic field localization near the surface of hemicylindrical particles. *Opt Quantum Electron*. 2018;50(11):1–8.
33. Mahariq I. On the application of the spectral element method in electromagnetic problems involving domain decomposition. *Turk J Electr Eng*. 2017;25(2):1059–1069.
34. I Mahariq, Erciyas A. A spectral element method for the solution of magnetostatic fields. *Turk J Electr Eng*. 2017;25(4):2922–2932.
35. Khan A, Raouf A, Zarin R, Yusuf A. Existence theory and numerical solution of leptospirosis disease model via exponential decay law. *AIMS Math*. 2022;7(5):8822–8846.
36. Mandal M, Jana S, Nandi SK, Khatua A, Adak S, Kar TK. A model based study on the dynamics of COVID-19: Prediction and control. *Chaos Solitons Fractals*. 2020;136:109889.
37. Khan A, Zarin R, Ahmed I, Yusuf A, Humphries UW. Numerical and theoretical analysis of Rabies model under the harmonic mean type incidence rate. *Results Phys*. 2021;29:104652.
38. Pakistan Population 1950–2020. 2020 https://www.worldometers.info/world-population/pakistan-population. Accessed 8th 2020.
39. Sapoukhina N, Tyutyunov Y, Arditi A. The role of prey-taxis in biological control. *Am Nat*. 2003;162:61–76.